ACS APPLIED MATERIALS & INTERFACES

www.acsami.org
Research Article

Scalable WS_2-Graphene Hybrids for Ultralow NO_2 Concentration Detection

Shuja Bashir Malik, Fatima Ezahra Annanouch,* Carla Bittencourt, and Eduard Llobet

Cite This: ACS Appl. Mater. Interfaces 2025, 17, 31592−31603
Read Online

ACCESS | Metrics & More | Article Recommendations | Supporting Information

ABSTRACT: This work presents a facile approach for fabricating hybrid heterostructures of tungsten disulfide (WS_2), synthesized via atmospheric pressure chemical vapor deposition (APCVD) and commercial graphene. A simple airbrushing technique, with nitrogen (N_2) as the carrier gas, was employed to fabricate the sensors. The morphological and structural characterizations of the hybrid material revealed a sheet-like synthesis of edge-enriched 2D WS_2 decorated with multilayer graphene nanomaterial. The gas-sensing properties of the pristine and hybrid materials were evaluated for nitrogen dioxide (NO_2) at various operating temperatures. The hybrid sensor with a WS_2 to graphene ratio of 3:1 demonstrated exceptional sensitivity to ultralow NO_2 concentrations (10 ppb) at a remarkably low operating temperature of 100 °C, outperforming both the graphene and WS_2 counterparts. Additionally, the sensor's responses to CO, H_2, C_6H_6, and NH_3 were examined to assess its selectivity. The sensor was tested under different relative humidity conditions (RH at 25 °C; 25%, 50%, and 75%). The sensor response nearly doubled at RH = 50%, highlighting its potential for practical applications in selective NO_2 detection. The sensor responses eventually reached saturation at 75% RH. In addition, the manuscript provides a detailed discussion of the NO_2 gas sensing mechanism.

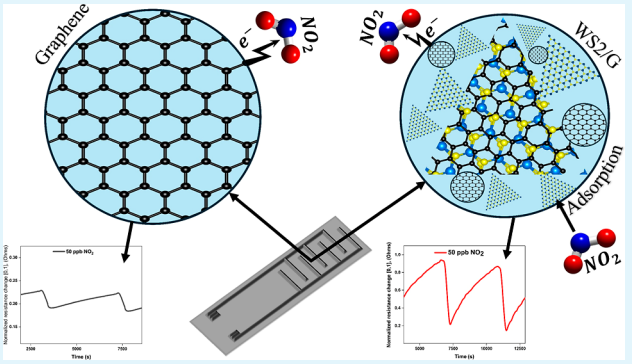

KEYWORDS: *WS_2, APCVD, sulfurization, gas sensor, NO_2, TMDs, 2D materials*

INTRODUCTION

Rapid industrial growth and population increase have remarkably elevated the emission of toxic gases and volatile organic compounds (VOCs) into the atmosphere, leading to life-threatening situations.[1] The main contributors to severe respiratory issues, including chronic bronchitis, respiratory irritation, and asthma, are parts per million (ppm) levels of NH_3 and parts per billion (ppb) levels of NO_2.[2,3] Common sources of these pollutants include power plant exhausts, industrial emissions, vehicular exhausts, and fertilizer production.[4,5] Additionally, NO_2 reacts with ambient compounds, leading to the formation of acid rain and ozone, thus exacerbating air pollution concerns.[4,6]

The United States Environmental Protection Agency (EPA) underscores the adverse effects of prolonged exposure to NO_2, noting that concentrations as low as several hundred parts per billion (ppb) can induce eye and lung irritation. To address these impacts, the EPA has established a long-term exposure limit of 53 ppb for NO_2.[7,8] It becomes imperative to identify and quantify the atmospheric concentrations of NH_3 and NO_2 to safeguard chemical processes, monitor human health, and ensure protection against gas leakage and chemical disasters.[2] Therefore, developing gas sensors with high sensitivity, selectivity, accuracy, reliability, and long-term stability is crucial for monitoring low concentrations of these hazardous gases.

Semiconductor gas sensors, particularly metal oxide-based sensors (MOX), have garnered tremendous attention due to their ease of fabrication, miniaturization, simple operation, and potential for mass production.[6] However, their performance is often constrained by a lack of selectivity and the requirement of high operating temperatures, which compromises stability and increases energy consumption.[6] While polymers offer an alternative due to their flexibility and ability to work at low temperatures, they often lack long-term stability under extreme conditions. In light of this, graphene has emerged as a promising candidate for gas sensing, exhibiting desirable intrinsic properties that surpass those of MOX and polymers. These properties include exceptional thermal conductivity (5000 W mK^{-1} at 27 °C),[9] high room-temperature carrier mobility (20,000 cm^2 V^{-1} s^{-1}),[10] low density (0.77 mg m^{-2}),[11] and remarkable chemical stability and mechanical durability (Young's modulus ∼1.02 TPa).[12] These attributes make graphene highly suitable for miniaturized, flexible gas sensors with superior sensitivity at low

Received: February 17, 2025
Revised: May 7, 2025
Accepted: May 8, 2025
Published: May 16, 2025

operating temperatures.[13] However, despite its advantages, graphene-based gas sensors still face challenges related to sensitivity, selectivity, and recovery speed.[14] Regardless of graphene's many promising qualities as a gas-sensing material, researchers are also exploring other two-dimensional materials for gas-sensing applications.[15]

Two-dimensional transition-metal dichalcogenides (2D TMDs), such as MoS_2 and WS_2, have attracted attention for their unique electrical, chemical, and optical properties.[16] They represent a promising class of layered van der Waals materials with excellent responses to hazardous gas species, especially NO_x.[13] Their large surface-area-to-volume ratios provide suitable adsorption sites for gas molecules, and the sensing mechanism is based on direct charge transfer upon gas adsorption.[9,10] However, pristine TMDs face challenges like low sensitivity at enhanced limits of detection (LoD), selectivity issues, and poor recovery.[11] Prolonged exposure of TMDs to atmospheric oxygen can accelerate oxidation, degrading sensing performance.[12] To address these limitations, functionalization strategies have been explored to enhance the performance of TMD-based sensors, with carbon-based materials like graphene being particularly promising. The synergistic effects of combining graphene and TMDs improve sensitivity, selectivity, and stability, making hybrid systems an effective solution for gas sensing applications,[17] The development of hybrids, particularly those combining graphene with other materials like metal oxides, MXenes, or TMDs, has emerged as an effective approach to enhance gas sensor performance at lower operating temperatures.[16] These hybrid systems offer the potential to address the limitations of pristine materials while taking advantage of their individual properties, especially for detecting gases at lower temperatures. Therefore, hybrid nanomaterials, especially the ones based on graphene and TMDs, represent a promising solution to overcome the inherent challenges faced by pristine materials, leading to high-performance gas sensors with lower energy consumption and better overall sensing capabilities. Concurrently, efforts are underway to explore the excellent properties of heterojunctions formed from different 2D materials such as graphene/WSe_2,[18] graphene/MoS_2,[19] graphene/$MoSe_2$,[20] or graphene/WS_2.[21] These heterojunctions exhibited excellent prospects for gas-sensing applications due to their enhanced electrochemical properties compared to their pristine counterparts.[22] Besides, diverse 2D layered nanomaterials are stacked to facilitate the regulation and manipulation of charge carrier generation, confinement, and transport.[23] A rational design of hybrids involves understanding the behavior of individual materials and exploiting their combined effects to enhance sensing behavior. Hao et al. investigated the adsorption of ten gas molecules on a graphene/WSe_2 heterostructure using first-principles calculations. The study revealed that NO_2 exhibited the strongest interaction with the heterostructure, acting as an electron acceptor and lowering the Schottky barrier height. Additionally, the application of a positive electric field (+0.5 V/Å) enhanced NO_2 sensitivity, offering insights for designing high-selectivity WSe_2-graphene based gas sensors.[18] This study also highlights the potential of graphene-TMD heterojunctions as efficient candidates for developing high-performance NO_2 gas sensors. According to the U.S. Environmental Protection Agency (EPA), the threshold limit value (TLV) for short-term exposure to NO_2 is 100 ppb, whereas long-term exposure is set at 53 ppb.[24]

Gas-sensing applications based on graphene and its derivatives often require additional modifications to enhance adsorption and electronic characteristics. Doping with various heteroatoms has been employed for this purpose.[25] Both graphene and its derivatives, such as reduced graphene oxide (rGO), demonstrate a distinct advantage in NO_2 gas detection due to their high carrier mobility and large surface-to-volume ratio.[25,26] Ma et al.[21] demonstrated self-powered photovoltaic flexible gas sensors through defect engineering controlled by ion irradiation employing a WS_2/graphene heterostructure. The graphene and WS_2 monolayers were grown via chemical vapor deposition which were then transferred to Si substrate employing wet-chemical processes. The sensors were able to detect as low as 50 ppb of NO_2. Graphene offers superior electrical conductivity and mechanical strength compared to reduced graphene oxide, making it more suitable for gas sensing applications, electronic devices, and advanced composites[27,28] Yan et al.[29] investigated the NO_2 sensing characteristics of WS_2/graphene aerogel (WS_2/GA) composites under varying humidity (0−60%) and temperature (RT to 180 °C). The WS_2/GA sensors demonstrated improved NO_2 selectivity compared to standalone graphene or WS_2 aerogels, with detection limits theoretically estimated to be 10−15 ppb. Optimum sensing performance was achieved at 180 °C in a dry atmosphere, while humidity enhanced response and recovery at room temperature, showcasing the composite's potential for adaptable gas sensing applications. Most of the reported works rely on synthesis techniques like hydrothermal synthesis and liquid phase exfoliation (LPE). However, these techniques suffer from challenges such as limited control over the size and quality of the produced materials, leading to variations in material properties. Moreover, the process often involves the use of hazardous solvents, posing environmental and safety concerns. Also, most of the reported methods for heterojunction fabrication involve the drop-casting method, where the thickness of the deposited film is seldom controlled.

Addressing the above-mentioned shortcomings, this work demonstrates an effective hybrid sensing material capable of detecting ultralow concentrations of NO_2. We present a methodology for fabricating WS_2/graphene hybrid thin films using a simple airbrush with WS_2 grown using the APCVD technique. The materials were directly deposited on the transducer substrates using an airbrushing technique with precise control over the thickness. The deposited materials were characterized for morphology, microstructure, phase, and chemical composition. The gas sensing properties of the films were studied toward low NO_2 concentrations at various operating temperatures (i.e., RT, 100 °C, and 150 °C) in both dry and humid conditions, as well as toward the interfering species like NH_3, CO, H_2, and C_6H_6. The hybrid material exhibited exceptional sensitivity to NO_2 with an experimental limit of detection (LoD) as low as 10 ppb, well within the EPA's threshold limits. This study highlights the potential of WS_2/graphene hybrids for advanced gas sensing applications, offering a reliable and scalable solution for monitoring hazardous gases.

EXPERIMENTAL SECTION

APCVD Synthesis of Sheet-Like WS_2. Atmospheric pressure chemical vapor deposition (APCVD) technique was used to synthesize sheet-like WS_2 with yield in hundreds of milligrams as reported in our earlier work.[30] The technique has the potential to be scaled to an industrial level. Commercially available tungsten trioxide powder procured from Sigma-Aldrich (CAS: 1314-35-8) was employed and sulfurized to obtain sheet-like WS_2 nanostructures in powder form. The sulfurization was carried out for 60 min at 900 °C using metallic sulfur (Sigma-Aldrich, CAS: 7704-34-9) in a homemade tube in tube furnace

https://doi.org/10.1021/acsami.5c03302
ACS Appl. Mater. Interfaces 2025, 17, 31592−31603

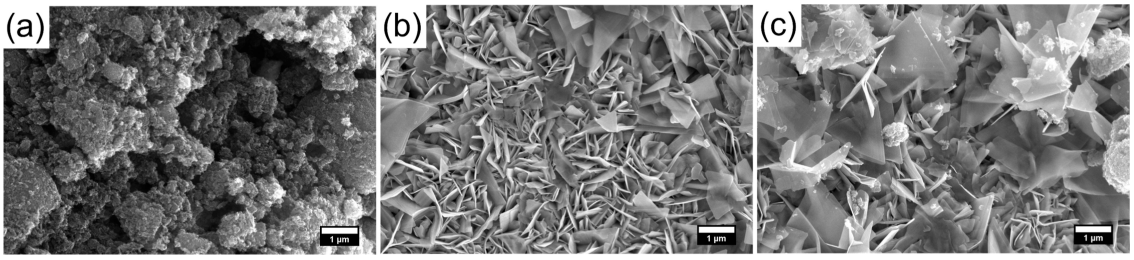

Figure 1. FESEM images of (a) graphene, (b) WS_2, and (c) WS_2/G1.

with a temperature gradient. The schematic of the furnace is shown in Figure S1. The middle zone of the furnace reaches a set temperature of 900 °C while the zones adjacent to the middle zone reach approximately 400 °C. Three alumina boats were positioned strategically within different temperature zones of the furnace; one boat contained 100 mg of WO_3 precursor powder, while the other two boats contained 1 g of sulfur each. One of the sulfur boats was placed adjacent to the WO_3-containing boat inside a semisealed secondary quartz tube, both situated in the 900 °C temperature zone. The reaction chamber was flushed with 100 mL/min of argon prior to sulfurization reaction, to remove oxygen present in the reactor. The boat outside the secondary quartz tube was placed upstream of argon flow inside the bigger quartz tube, Figure S1a. The argon flow was kept at 30 mL/min during the reaction. The furnace was programmed to reach the set temperature of 900 °C with a ramp of 40 °C/min. Upon reaching the set temperature (900 °C), the external quartz tube is carefully positioned such that the sulfur boat located outside the furnace is in the 400 °C temperature zone of the furnace, Figure S1b. This configuration ensures a sulfur-rich environment. The furnace was let to cool naturally after the completion of the reaction.

Pristine and -WS_2/Graphene Hybrids. Commercial graphene (CAS 1034343-98-0) was purchased from STREM Chemicals and was used to prepare sensors of pristine graphene and three hybrid combinations, with ratios of 3:1 and 1:1 of WS_2/graphene, respectively.

Gas Sensor Fabrication. Pristine graphene, WS_2, and WS_2/graphene hybrid sensing films were deposited on commercial alumina substrates (Ceram Tech GmBH, Germany) using a simple airbrushing technique. The alumina substrates have Pt-interdigitated electrodes with an electrode gap of 300 μm on the front side (2.5 mm × 5.1 mm) and a Pt-resistive heater meander on the back side. The substrates were cleaned with sequential sonication in acetone, ethanol, and deionized water, followed by nitrogen blow drying. The cleaned substrates were placed in a homemade airbrush system consisting of a hot plate, a commercial airbrush, a multimeter, and connectors.[30]

To deposit thin films of pristine graphene and pristine WS_2, 10 mg of graphene and WS_2 powder were separately sonicated in 10 mL of absolute ethanol (Scharlab, CAS: 64-17-5) for 1 h each, resulting in a black and brownish suspension, respectively. In the case of WS_2/graphene hybrids (WS_2/G), a constant total weight of 10 mg was maintained for both WS_2 and graphene. For hybrid WS_2/G1, 7.5 mg of WS_2 was mixed with 2.5 mg of graphene, while for hybrid WS_2/G2, 5 mg of WS_2 was mixed with 5 mg of graphene. The sensors are named WS_2/G1 and WS_2/G2, respectively. The amount of ethanol was kept constant at 10 mL in all the preparations, which were later transferred to an airbrush system. Preliminary experiments were conducted to evaluate various WS_2/graphene ratios, including 3:1, 1:1, 1:3, pristine WS_2, and pristine graphene; however, the 3:1 and 1:1 ratios demonstrated superior gas sensing performance, while the other compositions exhibited significantly lower sensitivity and were excluded from further analysis. The alumina substrates were placed on a hot plate kept at 55−60 °C, and the electrodes were connected to a multimeter in order to monitor, in real time, the resistance of the deposited films. This helps in achieving high reproducibility in the fabricated sensors. The solutions were airbrushed onto the alumina substrates using N_2 as a carrier gas.

Material Characterization Techniques. The characterization techniques employed in this study have been detailed in our previous work.[30] Briefly, the morphology of the materials was examined using Field Emission Scanning Electron Microscopy (FESEM, Thermo Scientific Scios 2). High-Resolution Transmission Electron Microscopy (HRTEM) was performed using a JEOL F200 TEM ColdFEG operating at 200 kV. TEM images were acquired using a Gatan OneView camera, a CMOS-based detector with a resolution of 4096 × 4096 pixels. The crystal structure of WS2 and the composite materials was analyzed by X-ray diffraction (XRD) using a Bruker-AXS D8-Discover diffractometer, equipped with a parallel beam geometry (Göbel mirror), vertical θ-θ goniometer, XYZ motorized stage, and a VÅNTEC-500 GADDS detector positioned 15 cm from the sample. The instrument operated at 40 kV and 40 mA to produce CuKα radiation. Raman spectroscopy was conducted using a Renishaw inVia spectrometer with a 514 nm argon-ion laser (Novatech, 25 mW). X-ray photoelectron spectroscopy (XPS) was performed with a PHI 5000 VersaProbe (Physical Electronics) using a monochromatic Al Kα source, with spectra recorded at a 45° takeoff angle. A spot size of 200 μm and a pass energy of 20 eV were used for core-level scans (W 4f, S 2p, C 1s). A dual beam charge neutralization system, combining an electron gun (<1 eV) and an argon ion gun (<10 eV), was applied to mitigate surface charging. Data analysis was carried out using CASA-XPS software.

Gas Sensing Measurements. The gas sensing measurements were performed using a homemade gas detection system consisting of a Teflon chamber with a net volume of 35 mL. The chamber consists of an inlet and outlet, which are connected to the gas delivery system and exhaust, respectively. A fully automated gas flow measurement system comprising mass flow controllers (MFCs, Bronkhorst High-Tech B.V.) was employed to supply the precise amounts of diluted gas mixtures. Calibrated gas cylinders balanced in dry synthetic air (Air Premier purity: 99.999%) were used for gas sensing measurements. The operating temperatures of the sensors were controlled by connecting the meander heaters of the sensors to an external power supply (Agilent U8002A). Sensor responses were recorded using an Agilent-34972A data acquisition system by monitoring the sensing material resistance changes upon exposure to different concentrations of target gases such as NH_3, NO_2, H_2, CO, and benzene. The sensor responses were evaluated at three different temperatures: room temperature (RT), 100 °C, and 150 °C. To ensure a stable baseline, a continuous flow of 100 mL/min of dry air was maintained in the chamber for 5 h prior to commencing the gas sensing experiments. The sensors were exposed to a specific gas species for 10 min, followed by a baseline recovery cycle, which was adjusted based on the sensor operating temperature: 60 min for 100 and 150 °C, and 120 min for RT operation. The overall flow of the dry air remained constant at 100 mL/min throughout the gas sensing measurements. The humidity effect on the sensing performance was evaluated by humidifying (at room temperature) the gas stream through a controller evaporator mixer from Bronkhorst. For oxidizing species like NO_2, the sensor response was calculated using eq 1, while for reducing species like NH_3, the sensor responses were calculated using eq 2.

$$R = \frac{R_{air} - R_{gas}}{R_{air}}^{*} 100 \quad (1)$$

https://doi.org/10.1021/acsami.5c03302
ACS Appl. Mater. Interfaces 2025, 17, 31592−31603

$$R = \frac{R_{gas} - R_{air}}{R_{air}}^{*} 100 \quad (2)$$

R_{air} and R_{gas} are the real time resistances of sensors when exposed to air and to target gas, respectively.

RESULTS AND DISCUSSION

Material Characterization. Field emission electron microscopy (FESEM) was conducted to study the structure and morphology of the materials. Bare graphene, as illustrated in the FESEM image in Figure 1a, reveals a multilayered, highly porous structure, which is desirable for gas sensing applications since it offers more active sites.[31] Figure 1b demonstrates pristine WS_2 with a distinct triangular sheet-like morphology. This peculiar triangular shape of WS_2 has been reported earlier as well.[32−35] The triangular morphology of WS_2 can be attributed to the fact that the crystal growth predominantly relies on the growth rates of two specific types of crystal faces, especially where the zigzag edge of tungsten or sulfur atoms terminate.[36,37] Upon in-depth analysis of the WS_2 using ImageJ software, it was found that the edge-to-edge width of the sheets is ∼700 nm, with the presence of some large sheets measuring around 1.5 μm with an average thickness of ∼40 nm. Figure 1c depicts the WS_2/G1 morphology. As is evident from the figure, the mixture of the two individual materials is uniform and homogeneous. FESEM image of WS_2/G2 is shown in Figure S2 in the Supporting Information.

X-ray diffraction (XRD) analysis was carried out to study the crystal structure of graphene, WS_2, and WS_2/G hybrids. The results are presented in Figure S3 as Supporting Information. All the peaks match well with the standard hexagonal phase of WS_2 (ICDD card number: 84-1398) with lattice constants a = 0.3152 nm and c = 1.232 nm belonging to the P63 space group. The diffractogram reveals the presence of intense peaks at 14.35°, 28.95°, 33.58°, 44.04°, 58.49°, 60.57°, 68.68° and 76.04° corresponding to (002), (004), (101), (006), (110), (112), (200) and (116) crystal planes. As can be seen from the diffractogram, the intense peak at 26.61° can be attributed to the (111) lattice phase of carbon corresponding to graphene (ICDD card number: 75-2078). Furthermore, minor peaks at 23.14°, 23.64°, and 24.36° corresponding to (002), (020), and (200) crystal planes of triclinic WO3 traces (ICDD card number 32-1395) were identified with lattice parameters a = 7.30 nm, b = 7.522 and c = 7.678 nm. Transmission electron microscopy (TEM) and high-resolution electron microscopy (HRTEM) were conducted to better understand the morphology and internal structure of the samples, respectively. Figure 2 shows an example of the obtained results for WS_2/G1. We can observe the presence of large, thin, and transparent WS_2 sheets stacked on top of each other with the presence of graphene as well. The insets in the figure show the interplanar distance of WS_2 and graphene. Upon further examination of the HRTEM images, the interplanar distances were determined to be 0.616 and 0.27 nm, corresponding to the (002) and (101) planes of WS_2 (ICDD card number: 84-1398). The inset, displaying the interplanar distance, d = 0.334 nm (111) plane, is attributed to graphene (ICDD card number: 75-2078). These results confirm the formation of the WS_2/G hybrid and agree with the XRD results. It is worth noting that similar results were observed from the other hybrid. Figure S4 depicts the HRTEM results of pristine graphene; it shows lattice fringes with interlayer spacing of 0.34 and 0.20 nm, indicative of pure multilayered graphene.

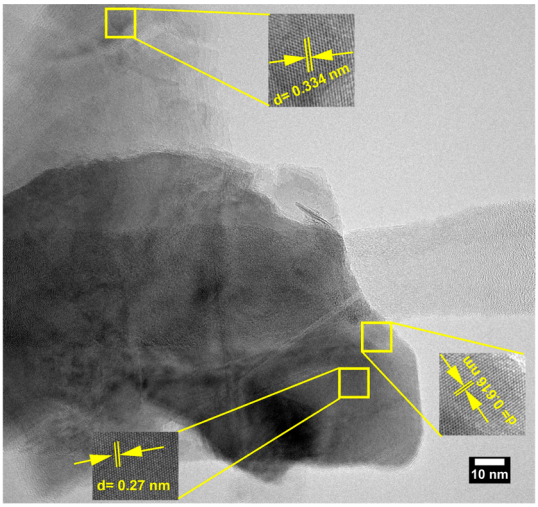

Figure 2. HRTEM image WS_2/G1.

Regarding pristine WS_2 samples, the obtained results are similar to the ones reported in our previous work.[30]

To study the accurate distribution of elements of WS_2/G1, EDS elemental mapping was conducted, as shown in Figure S5. The analysis confirms the presence of C, W, and S elements distributed uniformly over the WS_2 sheets. Also, Figure S5f shows the EDX spectra of the hybrid material with respective elements, confirming the high purity of the material.

Figure 3 displays an example of the spectrum obtained from WS_2/G1. It contains intense and sharp peaks, located at 352.7

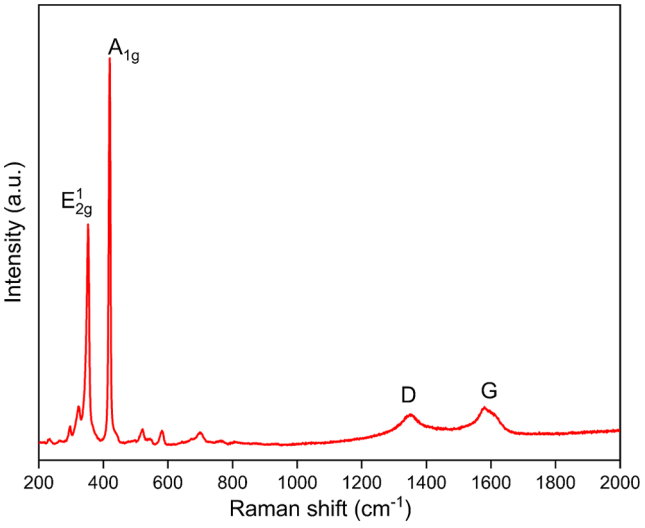

Figure 3. Raman spectra of WS_2/G1.

and 419.8 cm^{-1}, which correspond to E^1_{2g} and A_{1g} vibration modes of WS_2. The A_{1g} peak denotes the out-of-plane vibrational mode of S atoms and E^1_{2g} peak indicates vibration modes of W and S atoms. This confirms the formation of 2H phase-WS_2.[2] Also, the wavenumber difference between the Raman modes depends on the WS_2 film thickness. The difference between Raman shift of (A_{1g}−E^1_{2g}) is 67.1 indicating the composition of layered WS_2 film.[30,38] Also, the wavenumber difference between these modes (Δ = 67.1 cm^{-1}) and the broadening of the peaks are indicative of defect-rich WS_2, including S vacancies.[38] From the spectrum, the distinctive D

https://doi.org/10.1021/acsami.5c03302
ACS Appl. Mater. Interfaces 2025, 17, 31592−31603

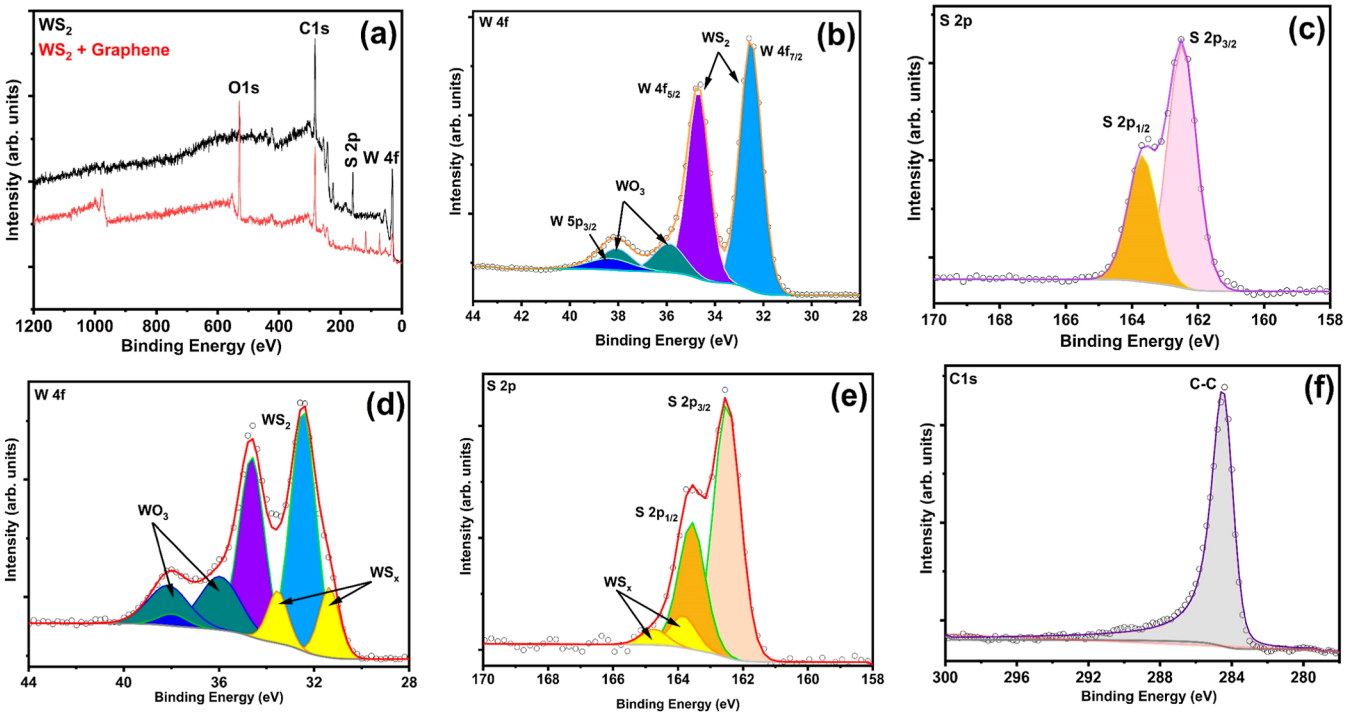

Figure 4. XPS spectra of WS_2 and WS_2 + graphene (WS_2/G1): (a) XPS survey scan, (b) W 4f core level of WS_2, (c) S 2p core level of WS_2, (d) W 4f core level of WS_2 + graphene, (e) S 2p core level of WS_2 + graphene, and (f) C 1s core level of WS_2 + graphene.

and G bands of graphene appear at approximately 1350 cm^{-1} and 1580 cm^{-1}, respectively. The D band, often associated with structural disorder or defects, arises from a hybridized vibrational mode linked to graphene edges. The G band results from first-order scattering of the E_{2g} mode within sp^2 carbon domains. The graphene exhibited an I_D/I_G value of 0.85, indicating a higher number of defects that facilitate gas adsorption,[39] which is desired for gas sensing applications. The Raman spectra of pristine graphene and pristine WS_2 are shown in Figure S6a,b, respectively.

X-ray photoelectron spectroscopy (XPS) was employed to investigate the chemical states and composition of both pristine WS_2 and WS_2/G1. The XPS survey spectra revealed the presence of W, C, S, and O in both samples, Figure 4a. A detailed analysis of the survey spectra of pure WS_2 indicates that 86% of the tungsten atoms participate in W−S bonding, with the remaining 14% associated with WO_3 impurities. The spectra recorded in the core-level binding energy regions allowed for the determination of the oxidation states of the elements.

For the pristine WS_2 sample, the W 4f binding energy region is well reproduced by one singlet and two doublets, as can be seen in Figure 4b. The singlet is centered at 38.4 eV, corresponding to the W $5p_{3/2}$ core level. The W $4f_{7/2}$ peaks associated with the two doublets are centered one at 32.5 eV, which corresponds to tungsten atoms in the W^{4+} valence state, and the other at 35.9 eV which corresponds to tungsten atoms in the W^{6+} valence state within WO_3.[35] The S 2p spectrum is characterized by the S $2p_{1/2}$ and S $2p_{3/2}$ peaks at 163.7 and 162.5 eV, respectively, with a spin−orbit energy separation of 1.2 eV, consistent with the S^{2-} oxidation state in WS_2, Figure 4c. Notably, the spectrum does not exhibit any discernible S−O bond component at 168.8 eV,[30,35] confirming the formation of WS_2 with minimal WO_3 impurities. Although the S 2s lines were initially referenced, this analysis highlights that the bonding environment of oxygen is exclusively associated with tungsten. The lower intensity of the S 2p peak and the absence of S−O bonds (which would appear at ∼168.8 eV) suggest the presence of S vacancies.[40]

For the graphene-loaded WS_2 sample (WS_2/G1), the XPS analysis revealed a higher relative concentration of carbon due to the addition of carbon nanostructures. The C 1s peak shows an asymmetric line characteristic of C−C sp^2 bonding, corresponding to the carbon nanomaterial (graphene), as is depicted in Figure 4f. In the W 4f binding energy region, an additional doublet with the W $4f_{7/2}$ component centered at 32.5 eV appeared compared to the pristine WS_2 sample, representing W−S bonding in WS_x, as can be seen in Figure 4d. This component accounts for 15% of the tungsten atoms, while 22% corresponds to WO_3 and 63% to WS_2. The S 2p spectrum of the graphene-loaded WS_2 sample does not exhibit any discernible S−O bond component at 168.8 eV,[41] Figure 4e. However, a low-intensity doublet attributed to WS_x was observed, indicating the presence of a minor phase of WS_x alongside the dominant WS_2 phase.[40]

Based on the XPS analysis, the graphene-loaded WS_2 sample (WS_2/G1) exhibits a complex chemical composition comprising of WS_2 (primary phase), WS_x with $x < 2$ (minor phase), and WO_3 (trace impurities), along with a sp2 bonded carbon (graphene). The analysis for the other hybrid sensor exhibits a similar composition, suggesting consistent formation of hybrid WS_2-based structures with graphene.

Gas Sensing Results. The gas sensing properties of graphene, WS_2, and WS_2/G hybrid sensors were tested for 50 ppb of NO_2 at various operating temperatures ranging from room temperature to 150 °C. It is worth noting that the operating temperature did not exceed 150 °C to avoid the evaporation of sulfur, which could deteriorate the sensing layer by forming a WO_3/WS_2 complex.[35] The optimal working temperature is an important parameter for evaluating overall sensor performance, impacting sensitivity, selectivity, response, and recovery speeds. Figure 5 shows the sensor responses of

https://doi.org/10.1021/acsami.5c03302
ACS Appl. Mater. Interfaces 2025, 17, 31592−31603

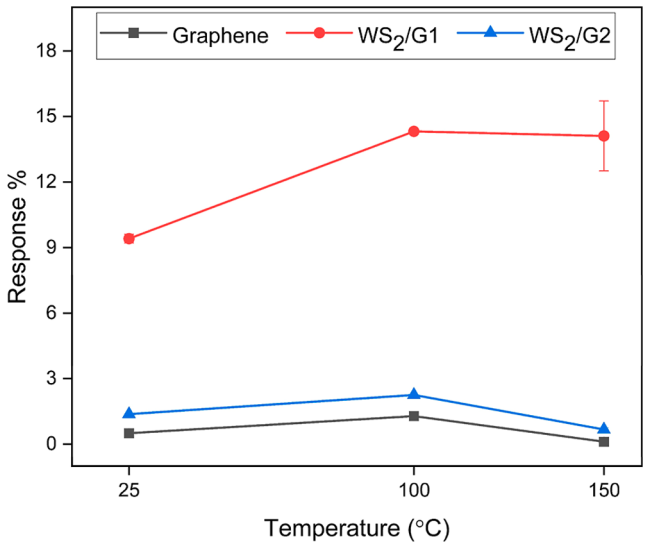

Figure 5. Sensor responses as a function of temperature toward 50 ppb of NO_2, graphene, WS_2/G1 and WS_2/G2.

graphene and WS_2/G1 and WS_2/G2 toward 50 ppb of NO_2 at different operating temperatures, ranging from RT (25 °C) to 150 °C. As illustrated, the sensor response increases from room temperature, peaks at 100 °C, and then decreases at higher temperatures. Thus, 100 °C was established as the optimal operating temperature for all subsequent studies. Notably, this working temperature is relatively low compared to that of metal oxide-based gas sensors.[6,42,43] It is worth mentioning that the pristine WS_2 sensor did not show any response to NO_2 at concentrations lower than 100 ppb. Therefore, it is not discussed.

In this study, the WS_2/G hybrid sensor demonstrated a significant enhancement in sensitivity, with the detection range decreasing from 100 to 10 ppb. This improvement can be attributed to the addition of graphene, which not only lowered the optimal operating temperature of the sensor but also facilitated enhanced electron mobility between the WS_2/graphene interface and the adsorbed analyte species.[44] Graphene offers high carrier mobility, a large specific surface area, and strong chemical stability.[44,45] The addition of graphene lowers the baseline resistance of the WS_2. These properties are advantageous for the WS_2/G hybrid sensor, as they increase the contact area, promote efficient charge transfer across the hybrid

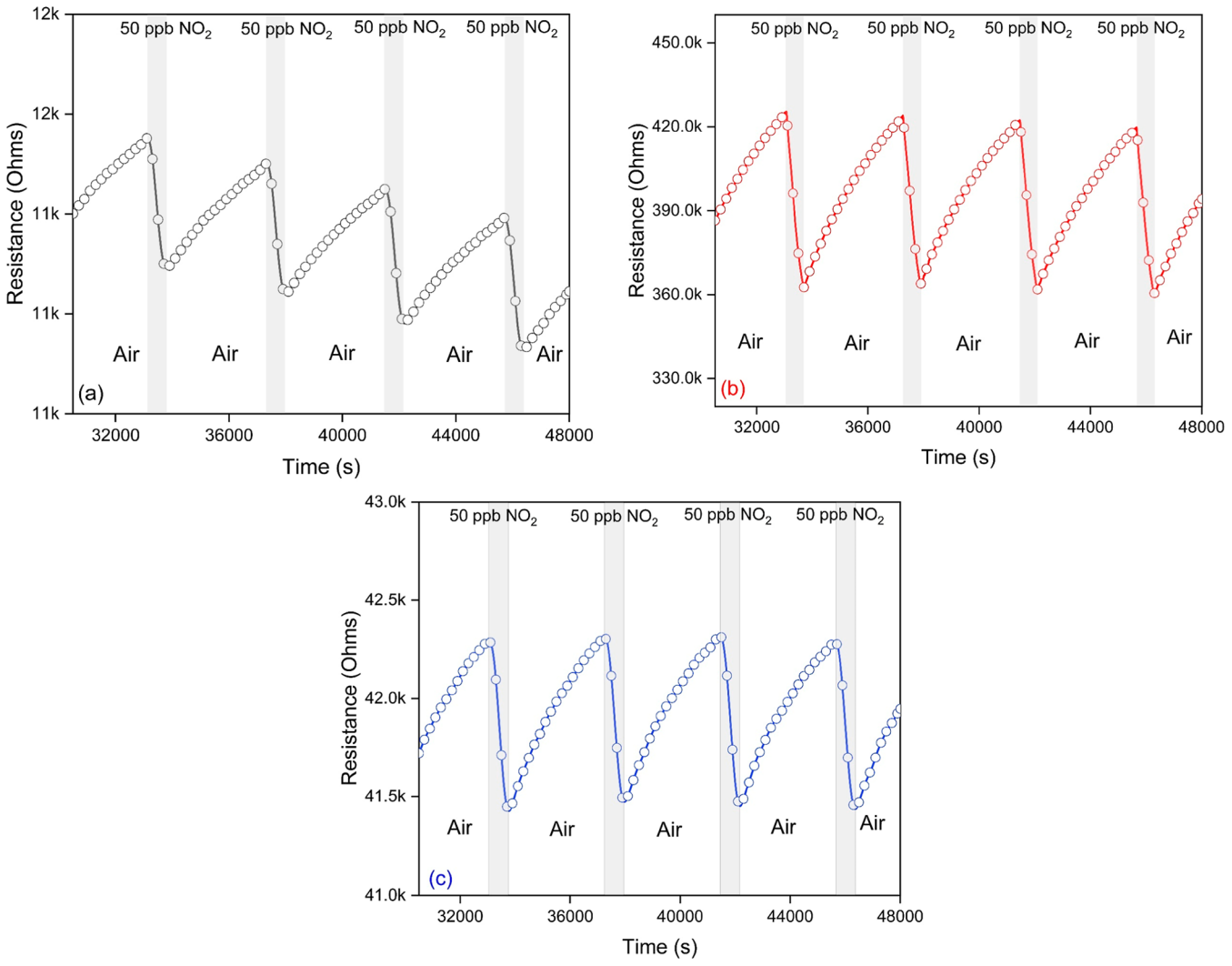

Figure 6. Dynamic resistance changes of (a) graphene, (b) WS_2/G1, and (c) WS_2/G2 toward 50 ppb of NO_2 at 100 °C.

https://doi.org/10.1021/acsami.5c03302
ACS Appl. Mater. Interfaces 2025, 17, 31592−31603

interface, and reduce charge transport time. The sp^2 carbon orbitals of graphene enable quick and efficient charge transfer,[35,46] offering substantial benefits for WS_2/G hybrid-based sensors by increasing the contact area and supporting effective charge transfer across the hybrid interfaces.

Figure 6 depicts the dynamic resistance changes of the pristine graphene, WS_2/G1, and WS_2/G2 sensors when exposed to 50 ppb of NO_2 while being operated at 100 °C. Upon being exposed to NO_2, an oxidizing gas species, the sensors respond as p-type semiconductors, showing a decrease in the resistance. This is in accordance with earlier research.[3,35] The decrease in resistance upon NO_2 exposure can be attributed to the spontaneous adsorption of NO_2 gas molecules on the sensing material surface. In this process, electrons are withdrawn via the valence band, leading to an increase in hole concentration and resulting in an overall decrease in the electrical resistance of the sensing film.[35,47,48] Moreover, when the target gas is removed during the recovery cycle, the sensors return completely to the original baseline resistance in a dry air environment.[42,43] The significant resistance change observed in WS_2/G1 can be attributed to the optimized 3:1 ratio of WS_2 to graphene, which enhances NO_2 adsorption and charge transfer efficiency. In contrast, pristine graphene exhibits a smaller resistance change due to the lack of active sites for NO_2 interaction, while WS_2/G2 (1:1 ratio) shows insignificant performance due to reduced active site density and less efficient charge transfer dynamics. The edge-enriched WS_2 nanosheets in WS_2/G1 further contribute to its superior sensing performance by providing abundant adsorption sites and facilitating strong interactions with NO_2 molecules. Additionally, we noticed a slight drift in the baseline resistance of pure graphene, suggesting the synergistic effect of WS_2 and graphene on the gas sensing properties and stability toward NO_2.

Pure graphene and WS_2/G2 exhibited responses of 1.28 ± 0.01% and 2.24 ± 0.03%, respectively, while WS_2/G1 displayed the highest response of 14.32 ± 0.04%, which is 11-times higher than the one of pristine graphene.

Moreover, the sensors were tested toward a wide range of NO_2 gas concentrations ranging from 10, 20, 30, 40, and 50 ppb at the optimal working temperature. Figure 7 shows the responses of the sensors as a function of the NO_2 concentrations. As it is evident from the figure, there is a linear increase in the response with the increase in the NO_2 concentration. As expected, the resistance changes recorded increase when the NO_2 concentration is also increased. The dynamics of the gas sensor film changes toward different NO_2 concentrations are presented in Figure S7. WS_2/G1 can efficiently detect as low as 10 ppb of NO_2. These detected concentrations are much lower than the permissible NO_2 concentrations.[49] Indeed, The American Conference of Governmental Industrial Hygienists (ACGIH) has established occupational guidelines for NO_2, suggesting a time-weighted average (TWA) of 3 ppm and short-term exposure limits (STEL) of 5 ppm. Meanwhile, the National Institute for Occupational Safety and Health (NIOSH) recommends a short-term exposure limit of 1 ppm over 15 min[49,50] Moreover, it can be seen from Figure S7a and c that there is no response from Pristine graphene and WS_2/G_2 sensors toward 10 ppb of NO_2. The relatively poor performance of the WS_2/G2 sensor is primarily due to the WS_2 to graphene ratio, which affects the charge transfer dynamics, the density of active sites, and the overall morphology of the hybrid material. We compared our sensor responses against the top-performing sensors reported in the literature, focusing on those utilizing TMDs and/or TMD-graphene composites. Remarkably, our sensors demonstrated superior performance across all evaluated parameters. Table S1 in the Supporting Information provides a detailed comparison, showcasing the exceptional NO_2 sensing characteristics of our sensors relative to other highly responsive TMD and TMD-graphene composite-based sensors.

Nevertheless, as the NO_2 concentration increases beyond 100 ppb, pristine WS_2 sensors start to exhibit an elevated response, surpassing that of all other sensors. These results are summarized in Figure 8, with an inset showing sensor responses across a range from 10 to 100 ppb NO_2. The sensing characteristics of pristine WS_2 emphasize its strong sensitivity to higher NO_2 concentrations (above 100 ppb). However, while pristine WS_2 shows a remarkable response at elevated concentrations, its sensitivity decreases at sub-100 ppb levels. In contrast, WS_2/G1 sensors address this limitation by detecting NO_2 at concentrations below 50 ppb, effectively minimizing

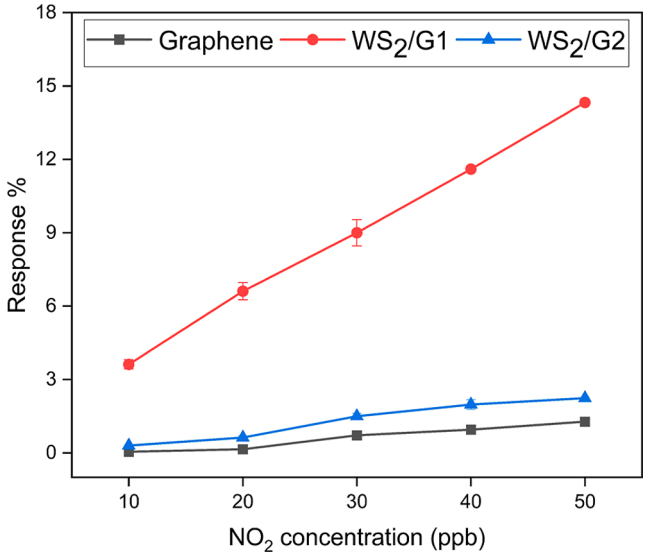

Figure 7. Sensor responses as a function of NO_2 concentration at 100 °C.

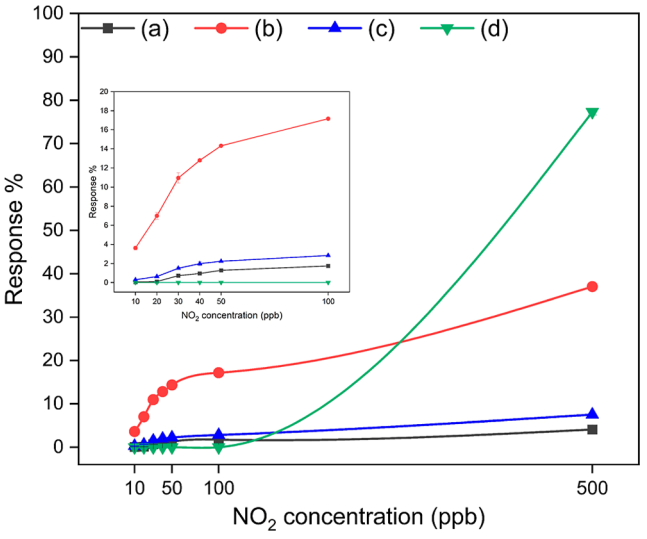

Figure 8. Sensor responses as a function of NO_2 concentration at 100 °C, (a) graphene, (b) WS_2/G1, (c) WS_2/G2 and (d) WS_2.

https://doi.org/10.1021/acsami.5c03302
ACS Appl. Mater. Interfaces 2025, 17, 31592−31603

cross-sensitivity issues. This improved limit of detection (LoD) in WS_2/G1 sensors improves the NO_2 LoD.

Selectivity is one of the important criteria for determining sensor performance. The selectivity of the sensors was evaluated toward fixed concentrations of various interfering species, viz. Carbon monoxide (CO), benzene (C_6H_6), ammonia (NH_3), and hydrogen (H_2) at the optimum working temperature of 100 °C. The fixed concentrations of the different gases were selected, keeping in view the permissible exposure limits of the respective analytes. Figure S8 shows the responses of the sensors toward the tested gases at 100. The results show that WS_2/G1 responds to an extremely low concentration of NO_2 (50 ppb) with the highest response of approximately 14%. The results suggest a high selectivity of the WS_2/G1 toward a meager NO_2 concentration of 50 ppb. All the gas concentrations tested are way below the permissible limits.[50] The combination of porous graphene and edge-enriched WS_2 particularly enhances sensitivity toward NO_2.[4]

The gas sensing properties of WS_2/G are significantly enhanced by the presence of defects in graphene. The defects in graphene are well demonstrated in Raman spectra (Figures 3 and S6). The graphene layer plays a crucial role in improving charge transfer between WS_2 and the target gas.[25] Furthermore, the presence of graphene (a layer in which charge carriers can move efficiently) enhances the collection of the generated charge carriers by the sensor device electrodes. Specifically, in the case of NO_2, the oxygen functional groups on WS_2 facilitate the adsorption of nitrogen dioxide molecules,[51] leading to the creation of more holes in the material and a subsequent decrease in sensor resistance. Pristine monolayer graphene, characterized by high electron mobility (2×10^5 cm^2 V^{-1} s^{-1}) and a large specific surface area (2630 m^2 g^{-1}),[52,53] exhibits distinct gas sensing properties.

The sensing characteristics of pristine WS_2 highlight its strong response to higher concentrations of NO_2 (above 100 ppb), where it demonstrates high sensitivity. When exposed to 5 ppm of NH_3 at 100 °C, pristine WS_2 sensors also show a significant response. Interestingly, even though the ammonia concentration is 100 times greater than that of NO_2, WS_2 sensors retain a preferential and selective sensitivity toward NO_2. This underscores the inherent specificity of WS_2 toward NO_2, even when exposed to a lower NO_2 concentration compared to NH_3. However, while pristine WS_2 shows a remarkable response for NO_2 at high concentrations, its responsiveness diminishes at sub-100 ppb levels. In contrast, the WS_2/G1 sensors address this limitation by detecting NO_2 concentrations below 50 ppb and thus effectively minimizing cross-sensitivity issues. This enhanced sensitivity observed in WS_2/G1 sensors improves the LoD for NO_2.

Sensing Mechanism. The sensing mechanism of graphene, WS_2, and WS_2/G is driven by charge transfer interactions between the sensing materials and the target gases.[54,55] NO_2 being an oxidizing gas, acts as an electron acceptor. When graphene is exposed to NO_2, the NO_2 molecules adsorb onto its surface and withdraw electrons. As a result, the hole concentration in p-type graphene rises, leading to a reduction in its resistance. In the case of pure WS_2, the multilayer structure provides abundant active sites accessible to the surroundings, facilitating efficient gas adsorption on exposed surfaces. Our earlier study demonstrated that the dominant interaction between gas molecules and WS_2 occurs through physisorption, accompanied by a moderate degree of electronic charge transfer.[30] Compared to pure WS_2, the hybrid structure has an even greater number of exposed active sites, leading to enhanced gas adsorption on the surface. This increased availability of active sites in the hybrid structure results in a higher response.

The layered architecture of WS_2/G enhances NO_2 adsorption and facilitates its diffusion through the interlayer spaces of the WS_2 nanosheets. Additionally, the ample WS_2 edge sites contribute significantly to NO_2 uptake and accelerate the reaction kinetics.[56] The porous architecture of WS_2/G provides a greater number of active sites on the graphene surface for NO_2 interactions. Moreover, the electron-deficient nature of WS_2 is effectively balanced by electron donation from graphene, facilitating charge transfer between the two components in the hybrid. This interaction induces notable change in the resistance in the WS_2/G composite, thereby enhancing its sensing performance as compared to individual WS_2 or graphene. Also, the work function of pristine graphene is 4.2 eV,[57,58] and that of WS_2 is 4.5 eV.[59] Due to the difference in work function between graphene and WS_2, electrons in graphene are preferentially transferred to the WS_2 nanosheets, leaving holes in graphene, thus, higher resistance changes and higher gas sensing responses.[60] As shown in Figure 6, the gas sensing response curves reveal that both graphene and WS_2/G exhibit p-type semiconductor behavior, characterized by a reduction in resistance upon exposure to NO_2. This resistance drop is attributed to electron withdrawal by NO_2 molecules. When the sensor is re-exposed to air, NO_2 molecules desorb from the surface, returning electrons to the sensing material and restoring its resistance to the initial baseline. The outstanding sensitivity and the ultralow detection limit observed can be attributed to the material's porous surface structure and the abundance of sulfur edge sites in WS_2, which result from the random three-dimensional stacking of WS_2 nanosheets.[35] Density functional theory (DFT) calculations demonstrate that edges on WS_2 enhance gas sensing performance.[30] Additionally, DFT calculations show that adsorption is weakest at the basal planes of WS_2 and highest at the edges. This stronger adsorption can induce a larger charge transfer compared to adsorption on the basal planes, thereby leading to remarkable sensitivity of WS_2/G. The proposed gas sensing mechanism is based on the adsorption/desorption of the gas molecules at the active sites of WS_2/G and is illustrated by the schematic sketch in Figure S9.

The capability of the WS_2/G material to detect ultralow concentrations of NO_2 can thus be mainly attributed to the following three factors. (i) Both the materials used in the hybrid are of high specific surface area ultimately leading to an increase in the average specific surface area. This, in turn, leads to a significant increase in the adsorption sites available, which increases the adsorption rate and, hence, gas response.[61] (ii) The hybrid formed consists of two materials with different Fermi levels. The formation of p−p heterojunction leads to an increase in the charge carrier mobility. (iii) The presence of defects, especially sulfur (S) vacancies in WS_2, leads to enhanced response toward NO_2.[41,62,63] These factors also help the sensing material to sense the ultralow concentrations of NO_2 in humid conditions.

Humidity Studies. To verify the practicability of the sensors, the impact of relative humidity on the sensor responses toward NO_2 was investigated. The sensors were tested toward 50 ppb of NO_2 at 100 °C in 25%, 50%, and 75% humidified air background. The results are summarized in Figure 9. The results indicate a clear trend in the sensing response corresponding to the varying humidity levels. At 25% RH, there was a noticeable increase in the sensing responses. When the relative humidity

https://doi.org/10.1021/acsami.5c03302
ACS Appl. Mater. Interfaces 2025, 17, 31592−31603

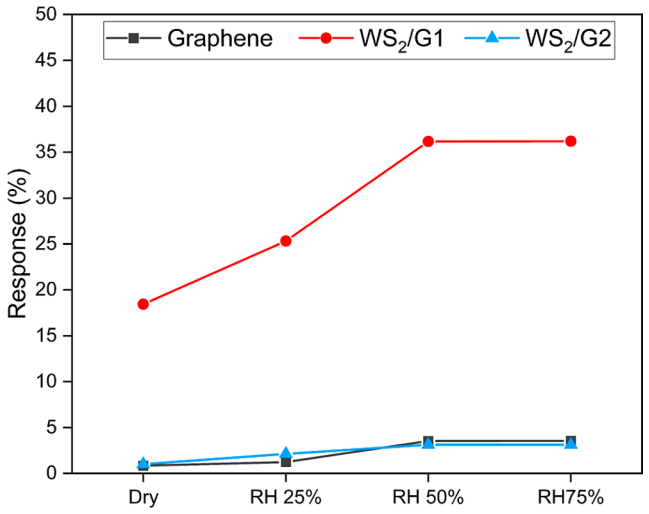

Figure 9. Dry and relative humidity cross-sensitivity to 50 ppb NO_2 at 100 °C.

was increased to 50%, the sensing response of WS_2/G1 was significantly enhanced, showing almost a 2-fold increase compared to the response at dry conditions, Figure S10. Interestingly, when the relative humidity was further elevated to 75%, the responses of the sensors were comparable to the responses observed at 50% RH. Figure S11a–c shows the dynamic resistance change of the sensors in a 50% humid and dry environment. It is observed that the sensor baselines increased under a humid environment. These results are in agreement with previously published results.[64,65] The increase in the baseline resistance under a humid environment could be explained on the basis of charge transfer between water molecules and the sensitive film. The adsorbed water molecules are known to behave like electron donors.[66,67] WS_2/G behaves as a p-type semiconducting material, and the increase in ambient humidity results in electronic charge (i.e., minority charge carriers) injected into the film, followed by recombination, which results in the reduction of hole density, leading to an increase in baseline resistance. In general, when testing sensors in a humid environment, there is competition between the target gas molecules and water vapor (hydroxyl groups) at the active sites. If the relative surface distribution of the hydroxyl group surpasses that of oxygen species, the sensor performance declines and the impact of humidity becomes more pronounced. Conversely, a sensor with strong resistance to moisture shows consistent performance, as adsorbed oxygen species occupy the majority of active sites. The influence of humidity on the sensor response highlights the need for humidity compensation to ensure reliable operation in real-world applications. Humidity affects the work function of the sensor by introducing water molecules that compete with NO_2 for adsorption sites and alter the baseline resistance. To address this, we propose several strategies for humidity compensation, including baseline correction, humidity-dependent calibration, and the integration of humidity sensors for real-time compensation.

Moreover, Figure S11d–f shows insets of the 10 ppb responses of the respective sensors, which are not observable under dry conditions. The increased responses in humid conditions and the stability of the response in a wide range of environmental humidity levels suggest that the WS_2/G sensors are excellent candidates for real-life applications.

CONCLUSION

This study highlights the potential of two-dimensional (2D) transition metal dichalcogenides (TMDs) for advanced low-temperature NO_2 gas sensing applications. APCVD was used as a high-yield synthesis method to synthesize edge-enriched WS_2. As synthesized, WS_2 was mixed with commercial graphene to form a WS_2/G hybrid to be used as a gas sensing material—a facile airbrushing technique with N_2 as the carrier gas was used to fabricate the sensors. The WS_2/G sensors demonstrate exceptional sensitivity to ultralow concentrations of NO_2 (10 ppb) at a notably low operating temperature of 100 °C, significantly outperforming their pristine WS_2 and graphene counterparts. Cross-sensitivity tests confirmed the negligible influence of interfering gases, including CO, H_2, C_6H_6, and NH_3, at the optimal working temperature of 100 °C, further emphasizing the sensor's excellent selectivity. Additionally, the sensor response was evaluated at 25%, 50%, and 75% RH, with results showing that the response nearly doubled at 50% RH, highlighting its strong potential for practical applications in selective NO_2 detection. The response reached saturation at 75% RH. This comprehensive approach lays the foundation for the development of highly efficient, selective, and scalable gas sensors capable of operating under real-world applications. The combination of TMDs and graphene, coupled with facile fabrication techniques, paves the way for next-generation gas sensing technologies, offering solutions to pressing environmental and industrial monitoring challenges.

ASSOCIATED CONTENT

Supporting Information

The Supporting Information is available free of charge at https://pubs.acs.org/doi/10.1021/acsami.5c03302.

Schematics of APCVD, FESEM image of graphene, XRD diffractograms; HRTEM images of graphene; Color mapping and EDS of WS_2/G1.; Raman spectra of pristine graphene ans pristine WS_2; resistance dynamics toward different NO_2 concentrations; selectivity graph, proposed sketch of sensing mechanism, humidity data, comparison table with literature (PDF)

AUTHOR INFORMATION

Corresponding Author

Fatima Ezahra Annanouch – *School of Engineering, Universitat Rovira i Virgili, MINOS, Tarragona 43007, Spain; IU-RESCAT, Research Institute in Sustainability, Climatic Change and Energy Transition, Universitat Rovira i Virgili, Vila-seca 43480, Spain; TecnATox - Centre for Environmental, Food and Toxicological Technology, Universitat Rovira i Virgili, Tarragona 43007, Spain;* orcid.org/0000-0003-1533-6482; Email: fatimaezahra.annanouch@urv.cat

Authors

Shuja Bashir Malik – *School of Engineering, Universitat Rovira i Virgili, MINOS, Tarragona 43007, Spain; IU-RESCAT, Research Institute in Sustainability, Climatic Change and Energy Transition, Universitat Rovira i Virgili, Vila-seca 43480, Spain; TecnATox - Centre for Environmental, Food and Toxicological Technology, Universitat Rovira i Virgili, Tarragona 43007, Spain;* orcid.org/0000-0002-1960-8783

https://doi.org/10.1021/acsami.5c03302
ACS Appl. Mater. Interfaces 2025, 17, 31592–31603

Carla Bittencourt − *Chimie des Interactions Plasma-Surface (ChIPS), Research Institute for Materials Science and Engineering, University of Mons, Mons 7000, Belgium*

Eduard Llobet − *School of Engineering, Universitat Rovira i Virgili, MINOS, Tarragona 43007, Spain; IU-RESCAT, Research Institute in Sustainability, Climatic Change and Energy Transition, Universitat Rovira i Virgili, Vila-seca 43480, Spain; TecnATox - Centre for Environmental, Food and Toxicological Technology, Universitat Rovira i Virgili, Tarragona 43007, Spain;* orcid.org/0000-0001-6164-4342

Complete contact information is available at: https://pubs.acs.org/10.1021/acsami.5c03302

Notes

The authors declare no competing financial interest.

■ ACKNOWLEDGMENTS

S.B.M. is supported by Martí-Franquès Research grants Programme, Doctoral grants −2019, (2019PMF−PIPF-14). F.E.A. is a RYC2022-038111-I postdoctoral fellow from the Ramon y Cajal programme. E.L. is supported by the Catalan Institution for Research and Advanced Studies via the 2018 Edition of the ICREA Academia Award. This work is supported by the Agencia Estatal de Investigación (AEI) under grant no. PID2022-142451OB-C21and by AGAUR under grant no. 2021 SGR 00147. The HRTEM was partially funded by the operative program FEDER Catalunya 2014-2020 (IU16-015844). C.B. is research associate of FNRS-Belgium.

■ REFERENCES

(1) Doan, T. H. P.; Ta, Q. T. H.; Sreedhar, A.; Hang, N. T.; Yang, W.; Noh, J.-S. Highly Deformable Fabric Gas Sensors Integrating Multidimensional Functional Nanostructures. *ACS Sens* **2020**, *5* (7), 2255−2262.

(2) Sardana, S.; Debnath, A. K.; Aswal, D. K.; Mahajan, A. WS2 Nanosheets Decorated Multi-Layered MXene Based Chemiresistive Sensor for Efficient Detection and Discrimination of NH3 and NO2. *Sens. Actuators B: Chem* **2023**, *394* (May), 134352.

(3) Alagh, A.; Annanouch, F. E.; Youssef, K. A.; Bittencourt, C.; Güell, F.; Martínez-Alanis, P. R.; Reguant, M.; Llobet, E. PdO and PtO Loaded WS2 Boosts NO2 Gas Sensing Characteristics at Room Temperature. *Sens. Actuators B: Chem* **2022**, *364*, 131905.

(4) Alagh, A.; Annanouch, F. E.; Sierra-Castillo, A.; Haye, E.; Colomer, J. F.; Llobet, E. Three-Dimensional Assemblies of Edge-Enriched WSe2Nanoflowers for Selectively Detecting Ammonia or Nitrogen Dioxide. *ACS Appl. Mater. Interfaces* **2022**, *14* (49), 54946−54960.

(5) Izelaar, B.; Ripepi, D.; van Noordenne, D. D.; Jungbacker, P.; Kortlever, R.; Mulder, F. M. Identification, Quantification, and Elimination of NO x and NH 3 Impurities for Aqueous and Li-Mediated Nitrogen Reduction Experiments. *ACS Energy Lett.* **2023**, *8* (8), 3614−3620.

(6) Malik, S. B.; Mejia-Centeno, K. V.; Martínez-Alanis, P. R.; Cabot, A.; Güell, F.; Annanouch, F. E.; Llobet, E. Synergistic Effect of CeO2 Nanoparticles and WO3 Nanowires in Gas Sensing Applications. *Sens. Actuators B: Chem* **2024**, *400* (October 2023), 134879.

(7) Behi, S.; Casanova-Chafer, J.; González, E.; Bohli, N.; Llobet, E.; Abdelghani, A. Metal Loaded Nano-Carbon Gas Sensor Array for Pollutant Detection. *Nanotechnology* **2022**, *33* (19), 195501.

(8) Cai, L.; Zhang, X. Sodium Titanate: A Proton Conduction Material for Ppb-Level NO2 Detection with near-Zero Power Consumption. *J. Hazard. Mater.* **2024**, *462* (July 2023), 132781.

(9) Manzoor, S.; Talib, M.; Novikov, S. M.; Arsenin, A. V.; Volkov, V. S.; Mishra, P. Physisorption-Mediated Charge Transfer in TiS2 Nanodiscs: A Room Temperature Sensor for Highly Sensitive and Reversible Carbon Dioxide Detection. *ACS Sens* **2023**, *8* (9), 3435−3447.

(10) Kushwaha, A.; Kumar, R.; Goel, N. Chemiresistive Gas Sensors beyond Metal Oxides: Using Ultrathin Two-Dimensional Nanomaterials. *FlatChem.* **2024**, *43* (July 2023), 100584.

(11) Recum, P.; Hirsch, T. Graphene-Based Chemiresistive Gas Sensors. *Nanoscale Adv.* **2023**, *6* (1), 11−31.

(12) Shin, D.; Sohn, I.; Kim, J.; Nakazawa, T.; Lee, S.; Yoon, H.; Yoo, J.; Park, J.; Chung, S.; Kim, H. Defect-Selective Functionalization of 2D-WS 2 Nanofilms with Pt Nanoparticles for Enhanced Room-Temperature NO 2 Gas Sensing. *ACS Appl. Nano Mater.* **2023**, *6* (20), 19327−19337.

(13) Kumar, R.; Goel, N.; Hojamberdiev, M.; Kumar, M. Transition Metal Dichalcogenides-Based Flexible Gas Sensors. *Sensors Actuators A Phys.* **2020**, *303*, 111875.

(14) Kang, S. B.; Sanger, A.; Jeong, M. H.; Baik, J. M.; Choi, K. J. Heterogeneous Stacking of Reduced Graphene Oxide on ZnO Nanowires for NO2 Gas Sensors with Dramatically Improved Response and High Sensitivity. *Sens. Actuators B: Chem* **2023**, *379* (November 2022), 133196.

(15) Wu, P.; Li, Y.; Yang, A.; Tan, X.; Chu, J.; Zhang, Y.; Yan, Y.; Tang, J.; Yuan, H.; Zhang, X.; Xiao, S. Advances in 2D Materials Based Gas Sensors for Industrial Machine Olfactory Applications. *ACS Sens* **2024**, *9* (6), 2728−2776.

(16) Malik, S. B.; Annanouch, F. E.; Llobet, E. Pd-Nanoparticle-Decorated Multilayered MoS2 Sheets for Highly Sensitive Hydrogen Sensing. *Chemosensors* **2023**, *11* (11), 550.

(17) Nawaz, F.; Ali, M.; Ahmad, S.; Yong, Y.; Rahman, S.; Naseem, M.; Hussain, S.; Razzaq, A.; Khan, A.; Ali, F.; Al Balushi, R. A.; Al-Hinaai, M. M.; Ali, N. Carbon Based Nanocomposites, Surface Functionalization as a Promising Material for VOCs (Volatile Organic Compounds) Treatment. *Chemosphere* **2024**, *364* (August), 143014.

(18) Hao, G.; Zhou, R.; Lei, W.; Li, H.; Zhang, R.; Ye, X. NO2 Capture on Graphene/WSe2 Heterostructure with High Sensitivity and Selectivity Modulated by External Electric Field. *J. Phys. Chem. Solids* **2022**, *165*, 110684.

(19) Sakthivel, R.; Geetha, A.; Anandh, B. A.; Jagadeesan, V.; Ganesh, A. S.; Dineshkumar, J. Design of MoS 2/Graphene Heterostructure Thin Film Sensors for High Performance NO 2 Gas Sensor Applications. *J. Phys. Conf. Ser.* **2021**, *2070* (1), 012131.

(20) Rathi, K.; Pal, K. Fabrication of MoSe 2 − Graphene Hybrid Nanoflakes for Toxic Gas Sensor with Tunable Sensitivity. *Adv. Mater. Interfaces* **2020**, *7* (12), 2000140.

(21) Ma, X.; Cai, X.; Yuan, M.; Qu, Y.; Tan, Y.; Chen, F. Self-Powered and Flexible Gas Sensor Using Defect-Engineered WS2/G Heterostructure. *Sens. Actuators B: Chem* **2022**, *371* (May), 132523.

(22) Hou, X.; Wang, Z.; Fan, G.; Ji, H.; Yi, S.; Li, T.; Wang, Y.; Zhang, Z.; Yuan, L.; Zhang, R.; Sun, J.; Chen, D. Hierarchical Three-Dimensional MoS2/GO Hybrid Nanostructures for Triethylamine-Sensing Applications with High Sensitivity and Selectivity. *Sens. Actuators B: Chem* **2020**, *317* (May), 128236.

(23) Yu, H.; Dai, M.; Zhang, J.; Chen, W.; Jin, Q.; Wang, S.; He, Z. Interface Engineering in 2D/2D Heterogeneous Photocatalysts. *Small* **2023**, *19* (5), 1−30.

(24) Feng, G.; Wang, S.; Wang, S.; Wang, P.; Wang, C.; Song, Y.; Xiao, J.; Song, C. Ultra-Sensitive Trace NO2 Detection Based on Quantum Dots-Sensitized Few-Layer MXene: A Novel Convincing Insight into Dynamic Gas-Sensing Mechanism. *Sens. Actuators B: Chem* **2024**, *400* (PA), 134852.

(25) Niu, Y.; Wang, R.; Jiao, W.; Ding, G.; Hao, L.; Yang, F.; He, X. MoS2 Graphene Fiber Based Gas Sensing Devices. *Carbon N. Y.* **2015**, *95* (2), 34−41.

(26) Choi, J.; Kim, T.; Li, H.; Jung, H. T.; Zhao, D. Gas Sensors with Two-Dimensional RGO@COF Composite Materials for Fast NO2 Detection under Room Temperature. *ACS Appl. Mater. Interfaces* **2023**, *15* (37), 44119−44126.

(27) Tiwari, S. K.; Sahoo, S.; Wang, N.; Huczko, A. Graphene Research and Their Outputs: Status and Prospect. *J. Sci. Adv. Mater. Devices* **2020**, *5* (1), 10−29.
(28) Phiri, J.; Johansson, L.-S.; Gane, P.; Maloney, T. A Comparative Study of Mechanical, Thermal and Electrical Properties of Graphene-Graphene Oxide- and Reduced Graphene Oxide-Doped Microfibrillated Cellulose Nanocomposites. *Compos. Part B Eng.* **2018**, *147* (November 2017), 104−113.
(29) Yan, W.; Worsley, M. A.; Pham, T.; Zettl, A.; Carraro, C.; Maboudian, R. Effects of Ambient Humidity and Temperature on the NO2 Sensing Characteristics of WS2/Graphene Aerogel. *Appl. Surf. Sci.* **2018**, *450*, 372−379.
(30) Malik, S. B.; Annanouch, F. E.; D'Souza, R.; Bittencourt, C.; Todorović, M.; Llobet, E. High-Yield WS 2 Synthesis through Sulfurization in Custom-Modified Atmospheric Pressure Chemical Vapor Deposition Reactor, Paving the Way for Selective NH 3 Vapor Detection. *ACS Appl. Mater. Interfaces* **2024**, *16* (36), 48585−48597.
(31) Casanova-Chafer, J.; Umek, P.; Acosta, S.; Bittencourt, C.; Llobet, E. Graphene Loading with Polypyrrole Nanoparticles for Trace-Level Detection of Ammonia at Room Temperature. *ACS Appl. Mater. Interfaces* **2021**, *13* (34), 40909−40921.
(32) Gutiérrez, H. R.; Perea-López, N.; Elías, A. L.; Berkdemir, A.; Wang, B.; Lv, R.; López-Urías, F.; Crespi, V. H.; Terrones, H.; Terrones, M. Extraordinary Room-Temperature Photoluminescence in Triangular WS 2 Monolayers. *Nano Lett.* **2013**, *13* (8), 3447−3454.
(33) Yue, Y.; Chen, J. C.; Zhang, Y.; Ding, S. S.; Zhao, F.; Wang, Y.; Zhang, D.; Li, R. J.; Dong, H.; Hu, W.; Feng, Y.; Feng, W. Two-Dimensional High-Quality Monolayered Triangular WS2 Flakes for Field-Effect Transistors. *ACS Appl. Mater. Interfaces* **2018**, *10* (26), 22435−22444.
(34) Jelken, J.; Avilés, M. O.; Lagugné-Labarthet, F. The Hidden Flower in WS2Flakes: A Combined Nanomechanical and Tip-Enhanced Raman Exploration. *ACS Nano* **2022**, *16* (8), 12352−12363.
(35) Alagh, A.; Annanouch, F. E.; Umek, P.; Bittencourt, C.; Sierra-Castillo, A.; Haye, E.; Colomer, J. F.; Llobet, E. CVD Growth of Self-Assembled 2D and 1D WS2 Nanomaterials for the Ultrasensitive Detection of NO2. *Sens. Actuators B: Chem* **2021**, *326*, 128813.
(36) Cheng, J.; Jiang, T.; Ji, Q.; Zhang, Y.; Li, Z.; Shan, Y.; Zhang, Y.; Gong, X.; Liu, W.; Wu, S. Kinetic Nature of Grain Boundary Formation in As-Grown MoS2Monolayers. *Adv. Mater.* **2015**, *27* (27), 4069−4074.
(37) Yan, J.; Lian, S.; Cao, Z.; Du, Y.; Wu, P.; Sun, H.; An, Y. CVD Controlled Preparation and Growth Mechanism of 2H-WS2 Nanosheets. *Vacuum* **2023**, *207* (September 2022), 111564.
(38) Iqbal, M. W.; Iqbal, M. Z.; Khan, M. F.; Shehzad, M. A.; Seo, Y.; Eom, J. Deep-Ultraviolet-Light-Driven Reversible Doping of WS2 Field-Effect Transistors. *Nanoscale* **2015**, *7* (2), 747−757.
(39) Wang, G.; Fan, J.; Xie, Y.; Yu, M.; Li, K.; Guo, X.; Wu, J.; Shi, K.; Pan, K. Monodisperse Y-Type CoO Hierarchical Nanostructure/Reduced Graphene Oxide for Improved NO2 Detection at Room Temperature with Enhanced Moisture Resistance. *Sens. Actuators B: Chem* **2023**, *394* (July), 134391.
(40) Shpak, A. P.; Korduban, A. M.; Kulikov, L. M.; Kryshchuk, T. V.; Konig, N. B.; Kandyba, V. O. XPS Studies of the Surface of Nanocrystalline Tungsten Disulfide. *J. Electron Spectrosc. Relat. Phenom.* **2010**, *181* (2−3), 234−238.
(41) Wang, X.; Gu, D.; Li, X.; Lin, S.; Zhao, S.; Rumyantseva, M. N.; Gaskov, A. M. Reduced Graphene Oxide Hybridized with WS2 Nanoflakes Based Heterojunctions for Selective Ammonia Sensors at Room Temperature. *Sens. Actuators B: Chem* **2019**, *282* (May 2018), 290−299.
(42) Li, Q.; Zeng, W.; Li, Y. Metal Oxide Gas Sensors for Detecting NO2 in Industrial Exhaust Gas: Recent Developments. *Sens. Actuators B: Chem* **2022**, *359* (2), 131579.
(43) Zhu, L.-Y.; Ou, L.-X.; Mao, L.-W.; Wu, X.-Y.; Liu, Y.-P.; Lu, H.-L. Advances in Noble Metal-Decorated Metal Oxide Nanomaterials for Chemiresistive Gas Sensors: Overview. *Nano-Micro Lett.* **2023**, *15* (1), 89.
(44) Choi, M. S.; Nipane, A.; Kim, B. S. Y.; Ziffer, M. E.; Datta, I.; Borah, A.; Jung, Y.; Kim, B.; Rhodes, D.; Jindal, A.; Lamport, Z. A.; Lee, M.; Zangiabadi, A.; Nair, M. N.; Taniguchi, T.; Watanabe, K.; Kymissis, I.; Pasupathy, A. N.; Lipson, M.; Zhu, X.; Yoo, W. J.; Hone, J.; Teherani, J. T. High Carrier Mobility in Graphene Doped Using a Monolayer of Tungsten Oxyselenide. *Nat. Electron.* **2021**, *4* (10), 731−739.
(45) Yuan, L.; Chung, T. F.; Kuc, A.; Wan, Y.; Xu, Y.; Chen, Y. P.; Heine, T.; Huang, L. Photocarrier Generation from Interlayer Charge-Transfer Transitions in WS2-Graphene Heterostructures. *Sci. Adv.* **2018**, *4* (2), 1−10.
(46) Bradford, J.; Shafiei, M.; MacLeod, J.; Motta, N. Synthesis and Characterization of WS2/Graphene/SiC van Der Waals Heterostructures via WO3−x Thin Film Sulfurization. *Sci. Rep.* **2020**, *10* (1), 1−10.
(47) Jiménez-Cadena, G.; Riu, J.; Rius, F. X. Gas Sensors Based on Nanostructured Materials. *Analyst* **2007**, *132* (11), 1083.
(48) Fei, H.; Wu, G.; Cheng, W. Y.; Yan, W.; Xu, H.; Zhang, D.; Zhao, Y.; Lv, Y.; Chen, Y.; Zhang, L.; Ó Coileáin, C.; Heng, C.; Chang, C. R.; Wu, H. C. Enhanced NO 2 Sensing at Room Temperature with Graphene via Monodisperse Polystyrene Bead Decoration. *ACS Omega* **2019**, *4* (2), 3812−3819.
(49) Kailasa Ganapathi, S.; Kaur, M.; Shaheera, M.; Pathak, A.; Gadkari, S. C.; Debnath, A. K. Highly Sensitive NO2 Sensor Based on ZnO Nanostructured Thin Film Prepared by SILAR Technique. *Sensors Actuators, B Chem.* **2021**, *335* (2), 129678.
(50) California Division of Occupational Safety and Health Webpage *PERMISSIBLE EXPOSURE LIMITS FOR CHEMICAL CONTAMINANTS TABLE AC-1*; dpp 1−26.
(51) Moumen, A.; Konar, R.; Zappa, D.; Teblum, E.; Nessim, G. D.; Comini, E. Room-Temperature NO 2 Sensing of CVD-Modified WS 2 − WSe 2 Heterojunctions. *ACS Appl. Nano Mater.* **2023**, *6* (9), 7323−7329.
(52) Guo, J.; Ruan, B.; Zhu, J.; Dai, X.; Xiang, Y.; Zhang, H. Low-Threshold Optical Bistability in a Metasurface with Graphene. *J. Phys. D Appl. Phys.* **2017**, *50* (43), 434003.
(53) Zhang, L.; Khan, K.; Zou, J.; Zhang, H.; Li, Y. Recent Advances in Emerging 2D Material-Based Gas Sensors: Potential in Disease Diagnosis. *Adv. Mater. Interfaces* **2019**, *6* (22), 1−27.
(54) Cha, J.-H.; Choi, S.-J.; Yu, S.; Kim, I.-D. 2D WS 2 -Edge Functionalized Multi-Channel Carbon Nanofibers: Effect of WS 2 Edge-Abundant Structure on Room Temperature NO 2 Sensing. *J. Mater. Chem. A* **2017**, *5* (18), 8725−8732.
(55) Cho, S.-Y.; Kim, S. J.; Lee, Y.; Kim, J.-S.; Jung, W.-B.; Yoo, H.-W.; Kim, J.; Jung, H.-T. Highly Enhanced Gas Adsorption Properties in Vertically Aligned MoS 2 Layers. *ACS Nano* **2015**, *9* (9), 9314−9321.
(56) Xu, Y.; Xie, J.; Zhang, Y.; Tian, F.; Yang, C.; Zheng, W.; Liu, X.; Zhang, J.; Pinna, N. Edge-Enriched WS2 Nanosheets on Carbon Nanofibers Boosts NO2 Detection at Room Temperature. *J. Hazard. Mater.* **2021**, *411* (January), 125120.
(57) Casanova-Chafer, J.; Garcia-Aboal, R.; Atienzar, P.; Feliz, M.; Llobet, E. Octahedral Molybdenum Iodide Clusters Supported on Graphene for Resistive and Optical Gas Sensing. *ACS Appl. Mater. Interfaces* **2022**, *14* (51), 57122−57132.
(58) Kumar, P. V.; Bernardi, M.; Grossman, J. C. The Impact of Functionalization on the Stability, Work Function, and Photoluminescence of Reduced Graphene Oxide. *ACS Nano* **2013**, *7* (2), 1638−1645.
(59) Aggarwal, P.; Bisht, P.; Ghosh, A.; Gourishetty, A. K.; Chang, E. Y.; Mehta, B. R.; Singh, R. γ-Ray-Induced Surface-Charge Redistribution and Change of the Surface Morphology in Monolayer WS 2. *ACS Appl. Nano Mater.* **2023**, *6* (9), 7404−7413.
(60) Yang, M.; Wang, L.; Hou, T.; Li, Y. Controlling of the Electronic Properties of WS 2 and Graphene Oxide Heterostructures from First-Principles Calculations. *J. Mater. Chem. C* **2017**, *5* (1), 201−207.
(61) Hu, J.; Xiong, X.; Guan, W.; Chen, Y.; Long, H. Design and Construction of Core-Shelled Co3O4-CoFe2O4 Heterojunction for Highly Sensitive and Selective Detection of Ammonia. *Chem. Eng. J.* **2023**, *452* (P2), 139346.

(62) Alagh, A.; Annanouch, F. E.; Youssef, K. A.; Bittencourt, C.; Güell, F.; Martínez-Alanis, P. R.; Reguant, M.; Llobet, E. PdO and PtO Loaded WS2 Boosts NO2 Gas Sensing Characteristics at Room Temperature. *Sens. Actuators B: Chem* **2022**, *364* (2), 131905.
(63) Xu, Y.; Xie, J.; Zhang, Y.; Tian, F.; Yang, C.; Zheng, W.; Liu, X.; Zhang, J.; Pinna, N. Edge-Enriched WS2 Nanosheets on Carbon Nanofibers Boosts NO2 Detection at Room Temperature. *J. Hazard. Mater.* **2021**, *411*, 125120.
(64) Paolucci, V.; Emamjomeh, S. M.; Ottaviano, L.; Cantalini, C. Near Room Temperature Light-Activated WS2-Decorated RGO as NO2 Gas Sensor. *Sensors* **2019**, *19* (11), 2617.
(65) Guo, R.; Han, Y.; Su, C.; Chen, X.; Zeng, M.; Hu, N.; Su, Y.; Zhou, Z.; Wei, H.; Yang, Z. Ultrasensitive Room Temperature NO2 Sensors Based on Liquid Phase Exfoliated WSe2 Nanosheets. *Sens. Actuators B: Chem* **2019**, *300*, 127013.
(66) Ikram, M.; Liu, L.; Lv, H.; Liu, Y.; Ur Rehman, A.; Kan, K.; Zhang, W. J.; He, L.; Wang, Y.; Wang, R.; Shi, K. Intercalation of Bi2O3/Bi2S3 Nanoparticles into Highly Expanded MoS2 Nanosheets for Greatly Enhanced Gas Sensing Performance at Room Temperature. *J. Hazard. Mater.* **2019**, *363*, 335−345.
(67) Li, Y.; Song, Z.; Li, Y.; Chen, S.; Li, S.; Li, Y.; Wang, H.; Wang, Z. Hierarchical Hollow MoS2Microspheres as Materials for Conductometric NO2 Gas Sensors. *Sensors Actuators, B Chem.* **2019**, *282*, 259−267.

https://doi.org/10.1021/acsami.5c03302
ACS Appl. Mater. Interfaces 2025, 17, 31592−31603